

# Multiple Andreev Reflection Effect Spectroscopy of Underdoped $\text{NaFe}_{1-x}\text{Co}_x\text{As}$ Single Crystals

S. A. Kuzmichev<sup>a,b</sup>, I. V. Morozov<sup>c</sup>, A. I. Shilov<sup>b</sup>, E. O. Rakhmanov<sup>b,c</sup>, and T. E. Kuzmicheva<sup>b,\*</sup>

<sup>a</sup> Faculty of Physics, Moscow State University, Moscow, 119991 Russia

<sup>b</sup> Lebedev Physical Institute, Russian Academy of Sciences, Moscow, 119991 Russia

<sup>c</sup> Faculty of Chemistry, Moscow State University, Moscow, 119991 Russia

\*e-mail: kuzmichevate@lebedev.ru

Received March 18, 2023; revised March 18, 2023; accepted March 20, 2023

We study the structure of the superconducting order parameter in underdoped  $\text{NaFe}_{1-x}\text{Co}_x\text{As}$  pnictides with  $T_c \approx 19\text{--}21$  K related to the 111 family. Using incoherent multiple Andreev reflection effect spectroscopy of planar break junctions, we directly determine the magnitudes of the two microscopic superconducting order parameters: the small superconducting gap  $\Delta_S(0)$ , and possible edges of the large gap  $\Delta_L(0)$  having an anisotropy in the  $ab$  plane at  $T \ll T_c$ , the corresponding characteristic ratios, as well as their temperature dependences. Additionally, we detect features of the tunneling  $dI(V)/dV$  spectra in  $\text{NaFe}_{1-x}\text{Co}_x\text{As}$  at  $eV^* > 2\Delta_L(0)$ , those irrelative to superconducting state, and discuss their origin.

DOI: 10.1134/S0021364023600751

## 1. INTRODUCTION

The 111 family of alkali-metal based superconducting (SC) pnictides, with  $\text{LiFeAs}$  and  $\text{NaFeAs}$  representative members, attracts the attention of theoreticians and experimenters so far due to a set of unique properties that are not typical for other families of iron-based SC (for a review, see [1]).  $\text{NaFeAs}$  shows superconductivity even in a stoichiometric state. Under a partial substitution of Fe by transition metal [1], its critical temperature reaches a maximum  $T_c \approx 22$  K simultaneously with antiferromagnetism (AFM) and nematicity suppression. The Fermi surface consists of hole barrels around the  $\Gamma$  point of the first Brillouin zone, and electron barrels near the M point [2], where several SC condensates develop below  $T_c$ .

The difficulties in studying  $\text{NaFeAs}$  cause a lack of experimental data available to date: due to a rapid (in a few minutes) degradation of  $\text{NaFeAs}$  SC properties in a presence of even trace amounts of  $\text{H}_2\text{O}$  and  $\text{O}_2$ , the sample preparation and the experiment should be provided in a protective atmosphere. The magnitudes of the SC gaps in  $\text{Na}(\text{Fe},\text{Co})\text{As}$  were probed using surface techniques (angle resolved photoemission spectroscopy (ARPES), scanning tunneling spectroscopy), and bulk techniques (specific heat measurements): a two-gap superconductivity was observed with the range of the characteristic ratios  $2\Delta(0)/k_B T_c \approx 5\text{--}9$  and  $2.5\text{--}4.5$  for the large and the small SC gaps, respectively (see Fig. 6 in [1]). It is

interestingly to note that a valuable  $k$  space anisotropy of the large SC gap was resolved in ARPES probes of underdoped  $\text{Na}(\text{Fe},\text{Co})\text{As}$  [3], that unobserved by the same research group in overdoped crystals with similar  $T_c \approx 18$  K. This fact could point to the influence of the AFM phase to the SC properties.

The significant spread of the characteristic ratios of the SC gaps available in literature to date, obviously, is results from a lack of direct probes of the gap structure of  $\text{NaFeAs}$ . Here, using an incoherent multiple Andreev reflection effect (IMARE) spectroscopy of planar break-junctions, we have locally and directly determined the energy SC order parameters, their characteristic ratios to the  $T_c$  introduced in the Barden–Cooper–Schrieffer (BCS) theory, and temperature dependences. We suggest a realization of the nodeless anisotropic large SC gap in the  $k$  space. For the first time, we detect features of tunneling  $dI(V)/dV$  spectra, irrelative to the SC state properties.

## 2. EXPERIMENTAL DETAILS

Single crystals of  $\text{NaFe}_{0.979}\text{Co}_{0.021}\text{As}$  nominal composition were grown by crystallization from melt. All manipulations such as the NaAs precursor obtaining and initial mixture preparation, their storage and preparation of samples for subsequent measurements were performed in Ar-filled glove box with residual concentration of water and oxygen less than 0.1 ppm. Then, preliminarily synthesized 0.058 g CoAs and

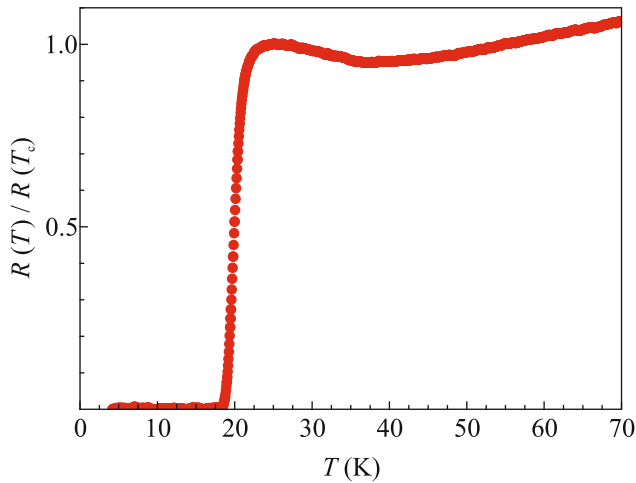


**Fig. 1.** (Color online) Temperature dependence of resistance of bulk  $\text{NaFe}_{0.979}\text{Co}_{0.021}\text{As}$  single crystal of nominally underdoped composition.

1.127 g Fe were added to 2.018 g of NaAs. The prepared reaction mixtures were placed in an alumina crucible, which was sealed in a niobium container in order to exclude a loss of alkali metal, then the niobium container was sealed in an evacuated quartz ampoule. The ampoule was heated up to  $1050^\circ\text{C}$  at a rate  $100^\circ\text{C}/\text{h}$ , and held at this temperature for 24 h. After it, the ampoule was cooled down to  $400^\circ\text{C}$  with a rate of  $3^\circ\text{C}/\text{h}$ , annealed at this temperature for 24 h, then cooled down in turned off oven to room temperature. The grown single crystals were extracted mechanically from the ingot using a Levenhuk DTX 700 microscope, then cut to proper plates size (typical size of the sample is 1.5–2.5 mm). Quantitative and qualitative composition of the grown crystals was confirmed by local X-ray microanalysis, and X-ray diffraction. The critical temperature of the bulk single crystals  $T_c \approx 21$  K was determined using resistive (Fig. 1) and magnetic measurements. Above  $T_c$ , the resistance of  $\text{NaFe}_{0.979}\text{Co}_{0.021}\text{As}$  bulk single crystal falls with temperature increase, reaches a minimum at the temperature of the structural transition  $T_s \approx 35$  K, whereas at higher temperatures  $R(T)$  shows a monotonic increase.

In order to form planar mechanically controlled nanoscale contacts of superconductor–constriction–superconductor (ScS) type with the current flowing along the  $c$ -direction, we used the planar “break junction” technique [4]. The configuration and the details of the experiment with layered samples, the advantages and disadvantages of the technique are discussed in [5]. A physical model of the typically obtained junction is schematically presented in Fig. 1 in [6].

Above  $T_c$ , the current through NcN junction (where N is a bulk normal metal), according to classical approach [7], is determined by the electron density

of states (DOS)  $N(E)$  energy distribution in the vicinity of the Fermi level  $E_F$  in metal:  $I \propto \int_{-\infty}^{\infty} N(\epsilon - eV)N(\epsilon)[f_0(\epsilon - eV) - f_0(\epsilon)]d\epsilon$ , where  $f_0$  is the equilibrium Fermi–Dirac function.

In the SC state, IMARE takes place in SnS junctions ( $n$  is thin normal metal) with NS interfaces of high transparency (the tunneling barrier strength  $Z \lesssim 0.3$ ). Incoherent Andreev transport causes an excess current in the current-voltage characteristic (CVC) of SnS junction (as compared to the normal-state CVC above  $T_c$ ) in the whole bias voltage  $eV$  range, whereas a supercurrent branch is absent [8, 9]. In the spectrum, at  $eV \rightarrow 0$  (so called foot area) dynamic conductance increases by several times relatively to the normal-state conductance  $G_N$  of the junction. As well, a series of subharmonic gap structure (SGS) dips appears in the  $dI(V)/dV$  spectrum, which positions  $V_n$  are directly determined by the SC gap  $\Delta$  at any temperature up to  $T_c$  [8–10]:  $|eV_n(T)| = 2\Delta(T)/n$ ,  $n = 1, 2, \dots$ . For a multiple-gap SC, the SGS of each gap would present in the  $dI(V)/dV$  spectrum. A number  $n^*$  of observable SGS dips for the planar junction roughly corresponds to the relation between the contact dimension  $d_c$  and the inelastic scattering length  $l_c$  along the  $c$ -direction [6, 9]:  $n^* \approx l_c/d_c$ .

In the planar SnS junction, in case of ballistic transport in the  $ab$  plane (if the mean free path  $l_{ab}^{\text{el}}$  exceeds  $d_{ab}$ ) both  $x$  and  $y$  components of the momentum of carriers are preserved, whereas the  $k_z$  component could be changed due to carrier “mixing” along the current direction resulting from inelastic scattering.

An influence of the  $\Delta(\theta)$  angle distribution in the  $k_x k_y$  plane ( $\theta$  is an angle in the basal plane) to the shape of Andreev dips in the framework of [11] is shown in Fig. 4 in [5]. Hypothetically, whereas sharp and intensive SGS dips are expected in the  $dI(V)/dV$  for an isotropic SC gap, but the SGS with a strongly suppressed intensity should be observed in case of nodal SC order parameter. In case of extended but nodeless  $s$ -wave gap symmetry in the  $ab$  plane, doublet SGS dips are expected, which width is determined by the maximum  $\Delta^{\text{out}}$  and the minimum  $\Delta^{\text{in}}$  Cooper pair coupling energies in the  $k$  space. Hereafter, the anisotropy degree is estimated as  $A \equiv 100\% \times [1 - \Delta^{\text{in}}/\Delta^{\text{out}}]$ .

In summary, IMARE spectroscopy of ballistic planar SnS junctions provides a direct determination of the values and temperature dependences of the SC order parameters, and to get some information about their possible anisotropy in the  $k_x k_y$  plane.

### 3. EXPERIMENTAL RESULTS AND DISCUSSION

In Fig. 2 the temperature evolution of the  $dI(V)/dV$  spectrum of SnS junction based on Na(Fe,Co)As is shown. In the normal state above  $T_c^{\text{local}} \approx 19.7$  K ( $T_c^{\text{local}}$  corresponds to a temperature at which the contact area with dimension about tens of nm transits to the normal state) the spectrum is strongly nonlinear: we observe a wide region of enhanced dynamic conductance at low bias voltages (foot), and dips at  $eV^* \approx 22, 27$  meV. With temperature increase from the lowest ones until  $T_c$ , the IMARE process suppresses, with it, zero-bias conductance  $G_{\text{ZBC}}$  at  $eV \rightarrow 0$  decreases. The dips at  $eV^*$  weakly shift toward zero bias. At temperatures higher than  $T_c$  (blue, cyan, and magenta curves in Fig. 2a), the  $G_{\text{ZBC}}$  value changes insignificantly (red circles in Fig. 2b).

Note that for SnS Andreev junction shown in Fig. 2 the observed nonlinear background of the  $dI(V)/dV$  spectrum cannot be caused by a local overheating of the junction by the measurement current since  $G_N(eV \gg 2\Delta)$  shown by green rhombs in Fig. 2 remains almost unchanged in the whole  $T$  range. In this Andreev junction, the heat should not be emitted in principle, since it initially was in the ballistic limit. One could easily ascertain it, checking the constancy of the  $G_{\text{ZBC}}$  value: indeed, it hardly changes at  $T > T_c$  (see red circles in Fig. 2b) as compared to the behavior of the conductance of the bulk single crystal (in accordance with  $R(T)$  shown in Fig. 1).

Additionally, the absence of heating in the obtained junction of high transparency could be checked as follows: in case of local overheating, due to a presence of diffusive transport the expression  $T^{\text{local}} \approx VL^{-1/2}/2$  ( $L$  is Lorenz number) is valid at bias voltages  $eV \gg k_B T$ , as a result, the observed normal-state conductance  $G_N$  of the junction would artificially depend on  $V$ . Using the experimental  $R(T)$  data (see Fig. 1), we simulated the conductance  $G^{\text{diff}}(V, T = 32.9$  K) of the diffusive junction (shown in the top of Fig. 2a by dashed line). Despite some similarity to the experimental spectrum measured at the same temperature (magenta curve) in the small bias voltage range, the  $G^{\text{diff}}$  behavior at  $V > V^*$  for the hypothetic diffusive junction strongly differs from that observed in the experiment.

The detected  $dI(V)/dV$  features do not directly relate to the SC state, since being observed above and below  $T_c$ . One could suggest several origins of such  $dI(V)/dV$  spectrum nonlinearity in the metallic state:

(a) nonlinear DOS  $N(E)$  distribution in the vicinity of  $E_F$  due to the band structure features in Na(Fe,Co)As (for example, Lifshitz transition or a minigap presence). In this case, the observed

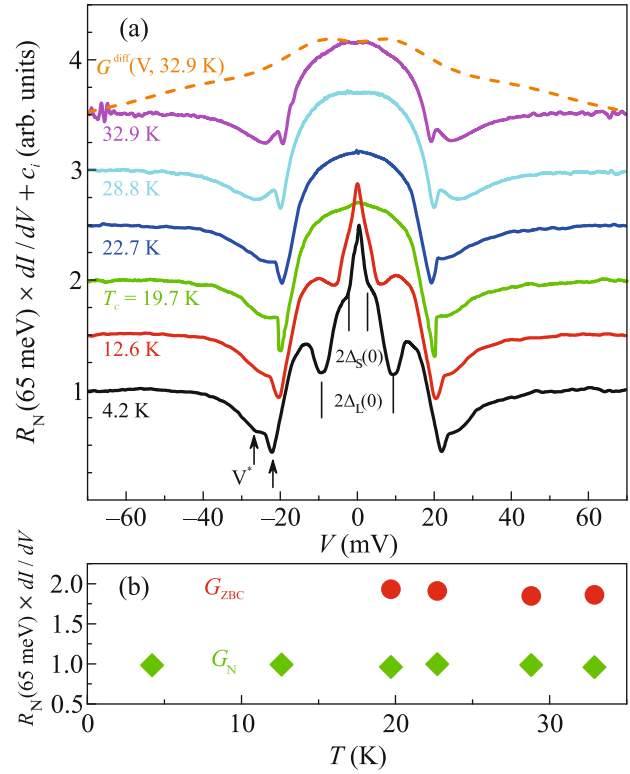


**Fig. 2.** (Color online) (a)  $dI(V)/dV$  spectrum of the SnS junction in Na(Fe,Co)As, measured above and below  $T_c \approx 19.7$  K. The curves are manually shifted by constant  $c = 0.5$  along the vertical axis for clarity. At 4.2 K, vertical dashes mark the position of the SC gap features ( $2\Delta_L(0)$ ,  $2\Delta_S(0)$ ), arrows point to the features of the normal-state conductance  $V^*$ . Dashed line corresponds to a theoretical spectrum  $G^{\text{diff}}(V)$  of fully diffusive junction at  $T = 32.9$  K, calculated using experimental  $R(T > T_c)$  from Fig. 1 in order to compare with upper magenta curve. (b) Constancy of the normal-state conductance of the junction  $G_N(T, V \gg 2\Delta_{L,S})$ , and its zero-bias conductance  $G_{\text{ZBC}}(T > T_c)$ .

$dI(V)/dV$  hump at  $eV \rightarrow 0$  corresponds to  $N(E)$  peak near  $E_F$ ;

(b) quasiparticle backscattering due to a strong electron-phonon interaction [12];

(c) electron DOS renormalization by a resonant interaction between electrons and characteristic bosonic modes those existing above  $T_c$  (for example, phonons, or nematic fluctuations).

In order to understand the origin of the nonlinearity of  $dI(V)/dV$  spectra of tunneling junctions in Na(Fe,Co)As in the normal state, further studies of its temperature and doping dependence are necessarily.

In the SC state, Andreev structures appear on the nonlinear  $dI(V)/dV$ -background: a sharp foot at  $eV \rightarrow 0$  and SGS dips produced by the large and the small SC gaps ( $2\Delta_L, 2\Delta_S$  labels in Fig. 2).

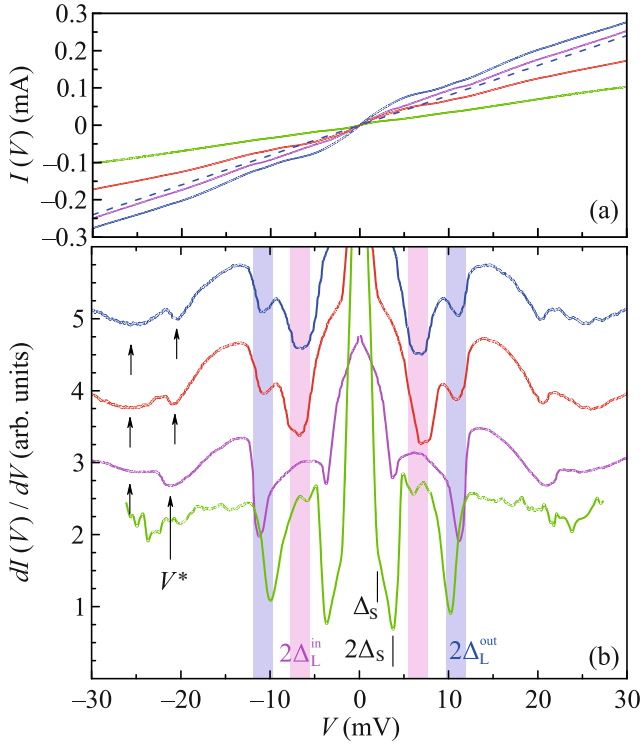


**Fig. 3.** (Color online) (a) Current–voltage characteristics and (b)  $dI(V)/dV$  spectra of SnS junctions with  $T_c^{\text{local}} \approx 19\text{--}21$  K, measured at 4.2 K. Arrows point to the normal-state conductance features  $V^*$ . Vertical areas mark the position of the fundamental Andreev dips that determine the energy parameters  $2\Delta_L^{\text{out}} \approx 10.8$  meV and  $2\Delta_L^{\text{in}} \approx 6.6$  meV (possibly, a doublet originated from the large SC gap with  $A_L \approx 39\%$  anisotropy in the momentum space), dashes show the  $n = 1, 2$  Andreev dips of the small SC gap  $2\Delta_S \approx 3.7$  meV. In (a) panel, the approximation for an ohmic dependence corresponding to  $G_N$  slope for the blue CVC is presented for comparison.

Figure 3 shows CVC and  $dI(V)/dV$  spectra within the bias voltage range  $\pm V^*$  of SnS junctions measured at 4.2 K. The junctions were formed in underdoped Na(Fe,Co)As single crystals with  $T_c \approx 19\text{--}21$  K from the same batch. Note the  $I(V)$  are symmetrical about zero, reproducibly show no hysteresis and supercurrent branch, which excludes Josephson nature of the observed  $dI(V)/dV$  features. Besides, CVC have an excess current within the whole  $eV$  range (compare solid and dashed blue curves in Fig. 3a), whereas a foot area at  $eV \rightarrow 0$  and Andreev dips are clear in the  $dI(V)/dV$  spectra. Such CVC and  $dI(V)/dV$  features correspond to IMARE regime and rather high transparency of SnS junction ( $Z < 1/2$ ), in accordance with all basic MARE models [8–10].

The features existing regardless to a presence of SC state and located at  $V^*$  bias are reproducibly observed

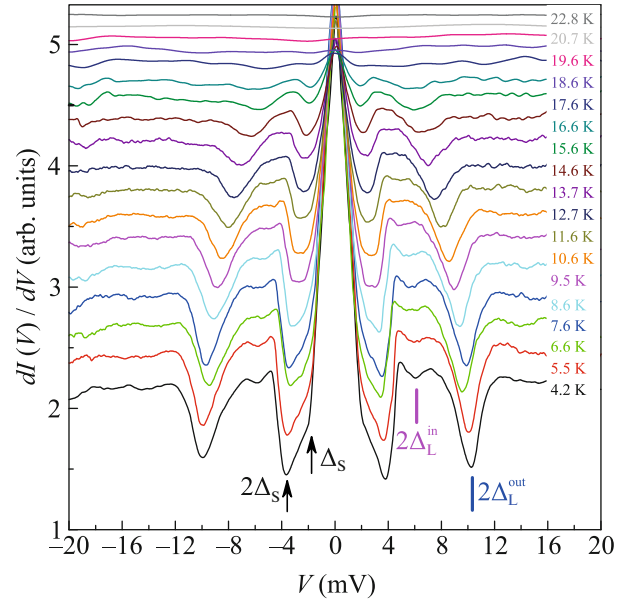


**Fig. 4.** (Color online) Temperature evolution of the  $dI(V)/dV$  spectrum of SnS junctions ( $T_c^{\text{local}} \approx 19$  K). The curves are manually shifted along the vertical axis, the normal-state nonlinear  $dI(V)/dV$  background is suppressed for clarity. The Andreev harmonics of SC order parameters  $\Delta_L^{\text{out}} \approx 5.1$  meV and  $\Delta_L^{\text{in}} \approx 3.1$  meV at 4.2 K are indicated by vertical lines, whereas those of  $\Delta_S \approx 1.9$  meV, by arrows.

in the spectra of various SnS junctions shown in Fig. 3b. At  $|eV| \approx 10.8$  meV and  $|eV| \approx 6.6$  meV, two Andreev dips are present. The ratio between their positions  $\approx 1.6$  does not correspond to  $n = 1, 2$  Andreev subharmonics of any isotropic SC gap, since  $V_1/V_2 = 2$ . Therefore, these two dips could form a doublet of fundamental ( $n = 1$ ) Andreev feature originated from an anisotropic SC gap, whereas its positions at  $T \ll T_c$  directly determine two characteristic energies of the SC order parameter  $\Delta_L^{\text{out}} \approx 5.4$  meV and  $\Delta_L^{\text{in}} \approx 3.3$  meV: the edges of possible Cooper pair coupling energy distribution on angle in the basal plane. The position of the doublet are reproducible in the  $dI(V)/dV$  spectra of various SnS junctions (see vertical magenta lines in Fig. 3b), do not depend on a *random* dimension of the contact area and its normal conductance  $G_N$  (therefore, the area of the junction). Thus, the doublet determines bulk SC order parameters Na(Fe,Co)As, and, therefore *cannot originate from dimensional resonances*. Similar doublets were reproducibly observed by us in a sister LiFeAs compound [13, 14], as well as in Ba(Fe,Ni)<sub>2</sub>As<sub>2</sub> pnictides (the 122 family) with close  $T_c$  [15–17].

The subharmonic gap structure of the small gap  $\Delta_S \approx 1.9$  meV is composed of minima located at lower bias voltages  $|eV| \approx 3.8$  meV ( $n = 1$ ) and 1.9 meV

( $n = 2$ ) (pointed to by vertical dashes in Fig. 3). Possibly, the suppressing of  $n > 1$  order subharmonics of  $\Delta_L^{\text{in,out}}$  is caused by their overlapping with the small gap SGS (since  $\Delta_L^{\text{out}} \approx 2.5\Delta_S$  at  $T \ll T_c$ ).

Temperature evolution of the  $dI(V)/dV$  spectrum of SnS junction is shown in Fig. 4. With temperature increase, the foot amplitude fades, Andreev dips become less intensive and shift toward zero bias in accordance with  $\Delta_i(T)$  temperature dependences. At  $T \approx 19.6$  K exceeding the local critical temperature of this junction  $T_c^{\text{local}}$ , as well as at higher  $T$ , CVC and  $dI(V)/dV$  spectrum show no features caused by IMARE transport, which corresponds to the contact area transition to the normal state (see upper spectra in Fig. 4).

Using data of Fig. 4, we directly measured the temperature dependences of the three observed energy gap parameters  $\Delta_L^{\text{out}}(T)$ ,  $\Delta_L^{\text{in}}(T)$ ,  $\Delta_S(T)$  (Fig. 5a). The dependences are typical for a moderate interband (crossband) coupling since their trends are similar, but pass a bit lower than a single-gap BCS-like behavior (dash-dotted line in Fig. 5a), which points to a realization of a multiple-gap SC state. The local critical temperature  $T_c^{\text{local}} \approx 18.8$  K for this contact was estimated as temperature at which  $\Delta_L^{\text{out}}, \Delta_S \rightarrow 0$ . The position of the Andreev feature labelled as  $\Delta_S$ , decreases more rapidly near  $T_c$  since the ratio  $\Delta_L^{\text{out}}/\Delta_S$  noticeably increases with temperature (Fig. 5b). Therefore,  $\Delta_S$  should be considered as a distinct SC order parameter, since Andreev features of the  $dI(V)/dV$  labelled as  $\Delta_S$  in Figs. 3, 4 cannot be subharmonics of  $\Delta_L^{\text{in,out}}$ . The  $\Delta_L^{\text{out}}(T)$ ,  $\Delta_L^{\text{in}}(T)$  dependences are generally the same, whereas  $A_L \equiv 100\% \times [1 - \Delta_L^{\text{in}}/\Delta_L^{\text{out}}] \approx 39\%$  ratio remains almost constant with temperature variation.

The observed doublets resemble those numerically calculated for a case of anisotropic SC gap (Fig. 4 in [5]) and therefore could be caused by a nodeless extended  $s$ -wave symmetry of the large SC gap  $\Delta_L$  in the  $k_x k_y$  plane. In this case,  $\Delta_L^{\text{out}}$  and  $\Delta_L^{\text{in}}$  correspond to the maximum and minimum Cooper pair coupling energies of the “leading” SC condensate in dependence of momentum direction. The supposed anisotropy degree  $A_L \approx 39\%$  is close to that estimated by us earlier for  $\Delta_L$  in  $\text{Ba}(\text{Fe,Ni})_2\text{As}_2$ ,  $\text{EuCsFe}_4\text{As}_4$  and  $\text{LiFeAs}$  [13–18], as well as to that observed by ARPES in underdoped  $\text{Na}(\text{Fe,Co})\text{As}$  [3].

The characteristic ratios  $r_i \equiv 2\Delta_i(0)/k_B T_c^{\text{local}}$  of the SC order parameters determined by us are  $r_L^{\text{out}} \approx 6.1$ ,  $r_L^{\text{in}} \approx 3.7$ , and  $r_S \approx 2.3 < 3.53$  (the latter is typical for “weak” or “driven” condensate in a multiple-gap SC).

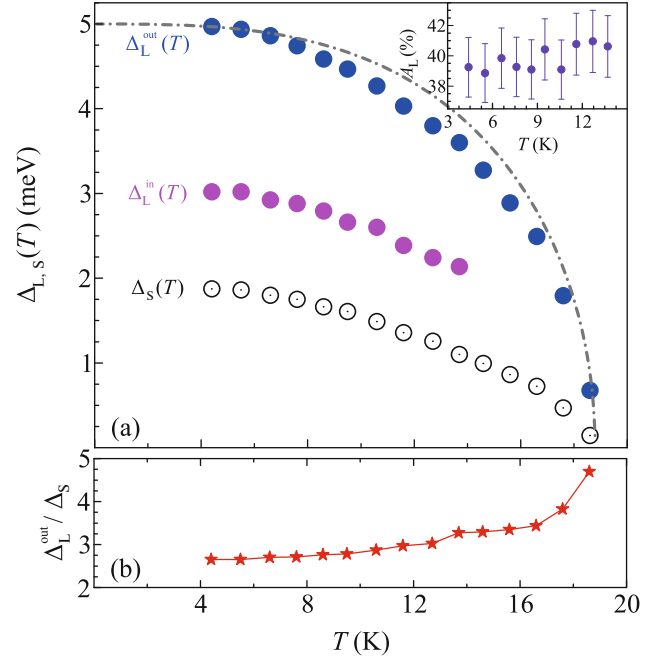


**Fig. 5.** (Color online) (a) Temperature dependences of the SC gap parameters  $\Delta_i(T)$ , obtained using data of Fig. 3. The inset shows the temperature dependence of possible anisotropy of the large SC gap  $A_L = 100\% \times [1 - \Delta_L^{\text{in}}/\Delta_L^{\text{out}}]$ . (b) Temperature dependence of  $\Delta_L^{\text{out}}(T)/\Delta_S(T)$  ratio. Dash-dotted line shows a single-gap BCS-like function.

On the other hand, comparing the obtained  $r_i$  ratios with the data by other groups (dashed areas in Fig. 6 in the review [1]), one could note that  $r_L^{\text{out}}$  is in the bottom of the range of the large gap characteristic ratios (blue dashing), whereas  $r_L^{\text{in}}$  values invade into the range of the small gap ratios (gray dashing in Fig. 6 in [1]). For this reason, we cannot exclude a coexistence of two distinct SC order parameters (labelled here as  $\Delta_L^{\text{in}}$  and  $\Delta_L^{\text{out}}$ ), developing at different Fermi surface sheets below  $T_c$ . In order to distinguish between the above mentioned cases and directly determine the symmetry type of  $\Delta_L$ , the available IMARE models [8–10] should be extended to be applicable for SC with anisotropic gap and elastic processes of carrier mixing (in the current direction), as well as more detailed studies of the shape of the doublets observed in the  $dI(V)/dV$  spectra of tunneling contacts.

#### 4. CONCLUSIONS

Using IMARE spectroscopy of planar ScS junctions in underdoped  $\text{Na}(\text{Fe,Co})\text{As}$  pnictides with  $T_c \approx 19\text{--}21$  K at temperatures above and below  $T_c$ , we detected a nonlinearity of the  $dI(V)/dV$  spectrum, that does not relate to the SC state. This nonlinearity

could originate from band structure features in the vicinity of  $E_F$ , or electron DOS renormalization due to a strong electron-boson interaction.

Below  $T_c$ , we directly determined the energy of the SC order parameters  $\Delta_L^{\text{out}}$ ,  $\Delta_L^{\text{in}}$ , and  $\Delta_S$  with the BCS characteristic ratios 6.1, 3.7, and 2.3, respectively.  $\Delta_L^{\text{out}}$  and  $\Delta_L^{\text{in}}$  could be either two distinct SC gaps developing at different Fermi surface sheets, or the edges of a single, anisotropic SC gap (maximum and minimum of the Cooper pair coupling energies angle distribution in the  $k$  space).

The  $\Delta_L^{\text{in,out}}(T)$  and  $\Delta_S(T)$  temperature dependences in Na(Fe,Co)As are typical for a moderate interband interaction, whereas the degree of the supposed large gap anisotropy  $A_L \approx 39\%$  remains almost unchanged with temperature variation.

#### ACKNOWLEDGMENTS

The work was partly carried out using the research equipment of the Shared Facility Center, Lebedev Physical Institute, Russian Academy of Sciences.

#### FUNDING

The work was supported by Russian Science Foundation project no. 22-72-10082.

#### CONFLICT OF INTEREST

The authors declare that they have no conflicts of interest.

#### REFERENCES

1. T. E. Kuzmicheva and S. A. Kuzmichev, JETP Lett. **114**, 630 (2021).
2. M. D. Watson, S. Aswartham, L. C. Rhodes, B. Parrett, H. Iwasawa, M. Hoesch, I. Morozov, B. Büchner, and T. K. Kim, Phys. Rev. B **97**, 035134 (2018).
3. Q. Q. Ge, Z. R. Ye, M. Xu, Y. Zhang, J. Jiang, B. P. Xie, Y. Song, C. L. Zhang, P. Dai, and D. L. Feng, Phys. Rev. X **3**, 011020 (2013).
4. J. Moreland and J. W. Ekin, J. Appl. Phys. **58**, 3888 (1985).
5. S. A. Kuzmichev and T. E. Kuzmicheva, Low Temp. Phys. **42**, 1008 (2016).
6. Z. Popovic, S. A. Kuzmichev, and T. E. Kuzmicheva, J. Appl. Phys. **128**, 013901 (2020).
7. I. Giaever and K. Megerle, Phys. Rev. **122**, 1101 (1961).
8. M. Octavio, M. Tinkham, G. E. Blonder, and T. M. Klapwijk, Phys. Rev. B **27**, 6739 (1983).
9. R. Kümmel, U. Günsenheimer, and R. Nicolisky, Phys. Rev. B **42**, 3992 (1990).
10. D. Averin and A. Bardas, Phys. Rev. Lett. **75**, 1831 (1995).
11. T. P. Devereaux and P. Fulde, Phys. Rev. B **47**, 14638 (1993).
12. I. K. Yanson, Sov. Phys. JETP **39**, 506 (1974).
13. T. E. Kuzmicheva, S. A. Kuzmichev, I. V. Morozov, S. Wurmehl, and B. Büchner, JETP Lett. **111**, 350 (2020).
14. S. Kuzmichev, T. Kuzmicheva, I. Morozov, A. Boltalin, and A. Shilov, SN Appl. Sci. **4**, 189 (2022).
15. T. E. Kuzmicheva, S. A. Kuzmichev, K. S. Pervakov, and V. A. Vlasenko, JETP Lett. **112**, 786 (2020).
16. T. E. Kuzmicheva, S. A. Kuzmichev, K. S. Pervakov, and V. A. Vlasenko, Phys. Rev. B **104**, 174512 (2021).
17. A. V. Sadakov, A. V. Muratov, S. A. Kuzmichev, O. A. Sobolevskiy, B. I. Massalimov, A. R. Prishchepa, V. M. Mikhailov, K. S. Pervakov, V. A. Vlasenko, and T. E. Kuzmicheva, JETP Lett. **116**, 708 (2022).
18. S. A. Kuzmichev, K. S. Pervakov, V. A. Vlasenko, A. Yu. Degtyarenko, S. Yu. Gavrilkin, and T. E. Kuzmicheva, JETP Lett. **116**, 723 (2022).